Discrimination Between Brown and White Adipose Tissue Using a 2-Point Dixon Water–Fat Separation Method in Simultaneous PET/MRI

Daniela Franz[1], Dimitrios C. Karampinos[1], Ernst J. Rummeny[1], Michael Souvatzoglou[2,3], Ambros J. Beer[2,3], Stephan G. Nekolla[2], Markus Schwaiger[2], and Matthias Eiber[2]

[1]Department of Diagnostic and Interventional Radiology, Technische Universität München, Munich, Germany; [2]Department of Nuclear Medicine, Technische Universität München, Munich, Germany; and [3]Department of Nuclear Medicine, Universität Ulm, Ulm, Germany

The purpose of the study was to evaluate signal-fat-fraction (SFF) analysis based on a 2-point-Dixon water–fat separation method in whole-body simultaneous PET/MR imaging for identifying brown adipose tissue (BAT) and discriminating it from white adipose tissue (WAT) using cross-validation via PET. **Methods:** This retrospective, internal review board–approved study evaluated 66 PET/MR imaging examinations of 33 pediatric patients (mean age, 14.7 y; range, 7.4–21.4 y). Eleven elderly patients were evaluated as controls (mean age, 79.9 y; range, 76.3–88.6 y). Pediatric patients were divided into 2 groups: with and without metabolically active supraclavicular BAT. The standard of reference for the presence of BAT was at least 1 PET examination showing ^{18}F-FDG uptake. PET/MR imaging included a 2-point Dixon water–fat separation method. Signal intensities in regions of interest on fat and water images and mean standardized uptake values (SUV_{mean}) were determined bilaterally in supraclavicular and gluteal fat depots. SFF was calculated from the ratio of fat signal over summed water and fat signal. Statistical analysis was conducted using the Student t test and correlation analysis. **Results:** SFF was significantly lower ($P < 0.0001$) in supraclavicular BAT than gluteal WAT in all pediatric subjects. Supraclavicular SFF was significantly higher in the control than in the pediatric group ($P < 0.0001$). In PET-positive patients with multiple examinations, SFF stayed stable whereas SUV_{mean} fluctuated (median intraindividual change, 5% vs. 91%). No significant correlation between SUV_{mean} and SFF could be observed for BAT. **Conclusion:** The results demonstrate that MR imaging–SFF analysis is a reproducible imaging modality for the detection of human BAT and discrimination from WAT. SFF values of BAT are independent from its metabolic activity, making SFF a more reliable parameter for BAT than the commonly used PET signal. However, with the intent to investigate both the composition of BAT and its activation status, hybrid PET/MR imaging might provide supplemental information.

Key Words: brown adipose tissue; signal-fat-fraction; simultaneous PET/MRI

Brown adipose tissue (BAT) is an organ responsible for thermogenesis through consummation of fat in response to certain stimuli such as low temperatures (1,2). BAT can be mostly found in supraclavicular and cervical depots in humans, whereas more anatomic sites (e.g., suprarenal, mediastinal) have been described in postmortem studies (3).

On a cellular level, in comparison to white adipose tissue (WAT), BAT is an extensively vascularized tissue characterized by smaller adipocytes than those in WAT, containing a centrally located nucleus, multiple triglyceride droplets, and a vast amount of iron-containing mitochondria and intracellular water (4). BAT can be found predominantly in babies and children, but several studies published during the last several years have demonstrated metabolically active BAT in adults (5–7). This finding corroborates observations of the aforementioned postmortem study that, even though there is an age relationship with BAT distribution, BAT is still present in adults (3). Notably, there is evidence that adults exhibit 2 types of BAT having the same cell morphology but originating from different progenitors (8).

The prevalence of obesity and its comorbidities is growing worldwide, leading to a global health issue and socioeconomic problem (9). Different studies have investigated BAT recruitment as a therapeutic approach for obesity, elevated triglyceride concentrations, and type 2 diabetes in rodents (10–13). Furthermore, studies in adult, pediatric, and adolescent populations showed an inverse correlation between obesity and the presence of metabolically active BAT determined by ^{18}F-FDG PET/CT examinations (6,14,15), rendering BAT an increasingly relevant role in the fight against obesity in humans (16–18). The development of precise and reliable tools for the quantification of body fat, its distribution, and determination of its type is highly needed. Several recent studies have investigated ^{18}F-FDG PET for identification of BAT, making PET/CT a reference modality in BAT imaging (7,14,19,20) in particular as it is depicting metabolic activity of BAT depots. Nevertheless, MR imaging is currently thought of as the best tool in the evaluation of body fat because of its detailed soft-tissue characterization, superior spatial resolution, and the lack of exposure for the patient to ionizing radiation (21,22). Therefore, MR imaging could represent an encouraging alternative to PET/CT to study BAT independently from its metabolic activity, especially in healthy populations.

Common parameters for the detection of BAT by MR imaging are the signal-fat-fraction (SFF) and the proton-density fat fraction
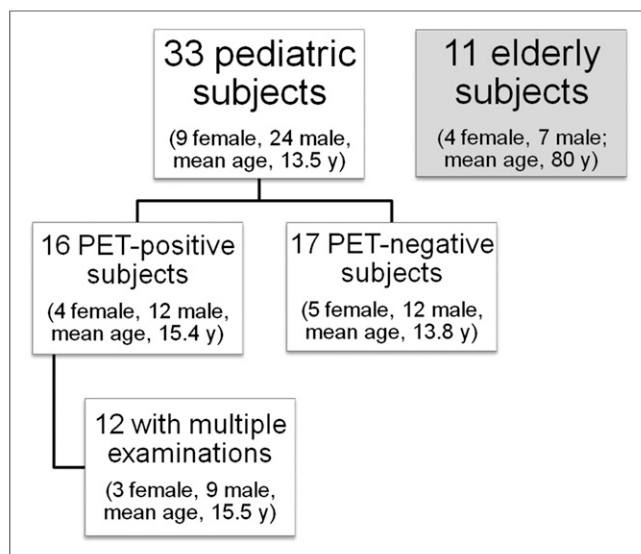
FIGURE 1. Age and sex of study and control cohorts (mean age at time of examination).

(PDFF), defined as the ratio of fat signal intensity over the sum of water and fat signal intensities. SFF and PDFF values reflect the different water content in BAT and WAT and have been approved in several studies (23–25). Some studies tried to relate the results of separate ^{18}F-FDG PET/CT and MR imaging examinations in a small number of patients proven to have metabolically active BAT on earlier ^{18}F-FDG PET/CT (26,27), evaluating metabolic activity and signal characteristics on MR imaging successively. Simultaneous ^{18}F-FDG PET/MR imaging represents a method to assess metabolic activity and MR imaging signal in a single examination without allowing interference by, for example, external factors such as cold exposition in between scans.

The present study is based on the hypothesis that MR imaging–SFF analysis is a reproducible imaging modality for the detection of human BAT and discrimination from WAT and that the presence of BAT is independent from BAT being metabolically active. A retrospective analysis using data from whole-body simultaneous ^{18}F-FDG PET/MR imaging studies in pediatric subjects based on a 2-point-Dixon water–fat separation method was pursued for identifying BAT with MR imaging and discriminating it from WAT using cross-validation via PET. Elderly subjects were chosen as a control group.

MATERIALS AND METHODS

Subjects

In a retrospective study, all pediatric subjects (age ≤ 21 y at the time of examination) who underwent ^{18}F-FDG PET/MR imaging due to oncologic diagnoses between September 2011 and April 2014 were retrieved from the institutional database. Institutional review board approval was obtained, and all subjects or their legal guardians gave informed assent/consent. Exclusion criteria were standard contraindications for MR imaging examinations.

Sixty-six ^{18}F-FDG PET/MR imaging examinations in 33 subjects were evaluated. The mean age of the pediatric subjects examined was 14.7 y (range, 7.4–21.4 y). The group of pediatric subjects was composed of 9 female individuals (mean age, 16.3 y; range, 9.5–21.4 y) and 24 male individuals (mean age, 14.1 y; range, 7.4–19.2 y) (Fig. 1). As a control group, ^{18}F-FDG PET/MR imaging data from 11 elderly

subjects (7 men, 4 women; mean age, 79.9 y; age range, 76.3–88.6 y) were evaluated. Exclusion criteria again were standard contraindications for MR imaging examinations. The mean injected activity of ^{18}F-FDG was 254 MBq (SD, 97; range, 75–471 MBq). Subjects fasted for 6 h before tracer injection, and blood glucose levels were measured just before injection, with a cutoff of 150 mg/dL. Sedation, which could potentially influence BAT activity (28), was not used in any patients.

Whole-Body Simultaneous ^{18}F-FDG PET/MR Imaging

All examinations were performed on a fully integrated whole-body hybrid system (Biograph mMR; Siemens Healthcare). ^{18}F-FDG PET/MR imaging was performed at a mean of 105 min after tracer injection (range, 63–175 min).

For all ^{18}F-FDG PET/MR imaging examinations, the following protocol was used. First, MR imaging localizer sequences were acquired to determine the location and number of PET bed positions. Second, the PET emission scans were initiated, with an emission time of 4 min per bed position. A 2-point T1-weighted coronal 3-dimensional Dixon spoiled gradient-echo sequence (volume-interpolated breath-hold examination [VIBE] Dixon sequence) combined with a water–fat separation method was acquired for attenuation-correction purposes simultaneously at the beginning of every PET measurement. To minimize motion artifacts from incomplete breath-holds, a centric k-space acquisition was used. Imaging parameters and setup for the spoiled gradient-echo sequence are summarized in Table 1. A water–fat separation was performed on the basis of the raw images, yielding 4 different image series: in-phase, opposed-phase, water-weighted, and fat-weighted. Depending on their oncologic diagnosis, further MR imaging sequences including at least a coronal T1-weighted turbo spin-echo sequence in all patients were acquired. All images were uploaded to a dedicated workstation (Syngo MMWP; Siemens Healthcare).

Image Analysis

Image datasets were analyzed by 2 experienced interpreters in consensus (2 and 8 y) who were masked to the patients' history.

To identify regions of BAT, the supraclavicular/cervical region was examined, because areas of adipose tissue can be easily identified and delineated in this area on anatomic images, and BAT in this region has been broadly characterized in PET/CT and autopsy studies (2,3,7,20). For areas of WAT, gluteal fat depots were evaluated because they are

TABLE 1
Technical Parameters of MR Sequence Used in Study

Sequence	T1-weighted VIBE Dixon
Repetition time/echo time (ms)	3.60/1.23–2.46*
Slice thickness (mm)	3.12
Gap (%)	0
Matrix	192 × 121
In-plane resolution (mm)	4.1 × 2.6
Field of view (mm)	500
% phase field of view	100
Acquisition time (min:s)	0:19
Number of excitations	1
Integrated parallel acquisition technique factor	2

*Fat-saturation techniques with Dixon require 2 repetition times.

TABLE 2
Overview of SFF and SUV_{mean} of PET-Positive, PET-Negative, and Control Group and *P* Values

Group	Supraclavicular			Gluteal			*P*
	Mean	SD	Range	Mean	SD	Range	
SFF							
PET-positive (*n* = 16)	0.70	0.08	0.50–0.88	0.92	0.04	0.84–0.97	<0.0001
PET-negative (*n* = 17)	0.76	0.1	0.32–0.94	0.91	0.04	0.81–0.97	<0.0001
Control (*n* = 11)	0.90	0.02	0.84–0.94	0.93	0.03	0.86–0.97	0.0026
SUV_{mean}							
PET-positive (*n* = 16)	4.0	4.77	0.29–19.75	0.20	0.09	0.08–0.50	<0.0001
PET-negative (*n* = 17)	0.45	0.17	0.24–0.91	0.20	0.09	0.02–0.44	<0.0001
Control (*n* = 11)	0.52	0.11	0.32–0.68	0.23	0.07	0.14–0.35	<0.0001

definable in every patient, and we expected to find exclusively WAT in the gluteal fat depots (*3,29*).

For every dataset with ^{18}F-FDG–avid supraclavicular fat depots, regions of interest (ROIs) were placed in the PET dataset bilaterally into the supraclavicular fat depots, automatically delineating the shape of the ^{18}F-FDG–avid fat depots (50% isocontour). If no or only low ^{18}F-FDG uptake could be detected, ROIs were placed into the fat-weighted MR image, automatically delineating the region with high signal on fat-weighted images—that is, the fat depot itself. For measurement of WAT, round ROIs were placed into gluteal subcutaneous fat depots bilaterally on the fat-weighted image.

The ROIs were automatically transferred to the coregistered images (fat-weighted and water-weighted images/water-weighted and PET images respectively). Mean signal intensities on fat- and water-weighted images and mean standardized uptake values (SUV_{mean}) of the PET dataset were noted. SFF for BAT and WAT was calculated using the following formula: $\frac{\text{fat signal intensity}}{(\text{fat signal intensity} + \text{water signal intensity})}$.

Finally, subjects were divided into 2 groups: the PET-positive group, with moderate to high ^{18}F-FDG uptake ($SUV_{mean} > 1$) in at least one ^{18}F-FDG PET examination, and the PET-negative group, with no or low uptake in all available examinations.

Statistical Analysis

Data are expressed as mean ± SD (with range in parentheses) if not otherwise denoted. An unpaired Student *t* test was used to compare the SFF and SUV_{mean} in supraclavicular/cervical and gluteal adipose tissue as well as to compare the SFF of the study group and the control group. Linear regression analysis was used to determine the correlation coefficient between SFF and SUV_{mean}. In all experiments, a probability value of less than 0.05 was considered significant. Statistical analysis was performed using MedCalc statistical software (version 7.2.0.2; MedCalc Software).

RESULTS

First, the numbers of PET-positive and PET-negative subjects were determined. Of the 33 examined pediatric subjects, 16 were found to have ^{18}F-FDG–avid, metabolically active supraclavicular/cervical fat depots in at least 1 of their examinations suggestive of BAT. Therefore, these subjects were determined as PET-positive. Of those 16 subjects, 12 had multiple examinations, resulting in 38 examinations. In all other pediatric subjects (*n* = 17, total number of 28 examinations) and the 11 subjects in the control group, no metabolically active adipose tissue was found (Fig. 1). Thus, these subjects were determined as PET-negative.

Within the group of PET-positive pediatric subjects, MR imaging–based mean SFF was 0.70 ± 0.08 in supraclavicular BAT (range, 0.5–0.88) and 0.92 ± 0.04 in gluteal WAT (range, 0.84–0.97). These values resulted in a highly significant difference between the 2 types of fat (*P* < 0.0001) (Table 2).

In the 12 PET-positive subjects with multiple examinations, intraindividual SFF in supraclavicular fat depots was relatively constant at all measurements, with a median percentage change of 5% (range, 0%–39%). In contrast, intraindividual changes in ^{18}F-FDG uptake were considerably higher, with a median difference of 91% for the SUV_{mean} (range, 10%–5,621%). In gluteal depots, median change in SFF was 2% (range, 0%–9%) whereas median change in SUV_{mean} was 39% (range, 0%–117%). SFF and SUV_{mean} in supraclavicular and gluteal fat depots of all examinations in the PET-positive subjects are shown in Figure 2. Because of this relatively stable SFF and highly variable SUV_{mean}, no correlation between SFF in supraclavicular fat depots and SUV_{mean} could be found (*r* = −0.125; *P* = 0.304).

Within the group of PET-negative pediatric subjects, MR-based mean SFF was 0.76 ± 0.1 in supraclavicular depots (range, 0.32–0.94) and 0.91 ± 0.04 in gluteal fat tissue (range, 0.81–0.97), also resulting in a highly significant difference (*P* < 0.0001) (Table 2).
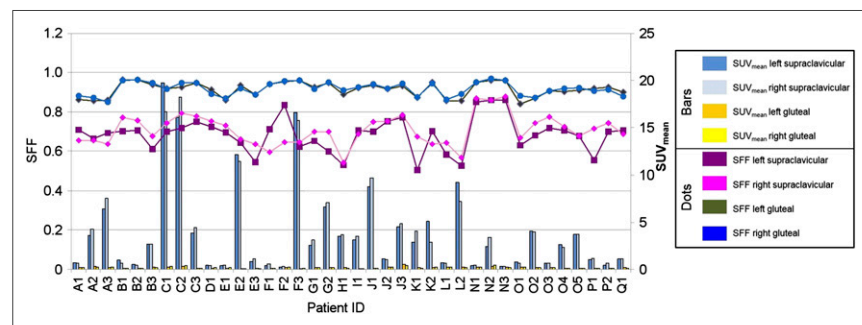

FIGURE 2. SFF and SUV_{mean} in supraclavicular and gluteal fat depots in PET-positive subjects. Each patient is represented by specific letter. In patients with multiple examinations, number displays individual examination.
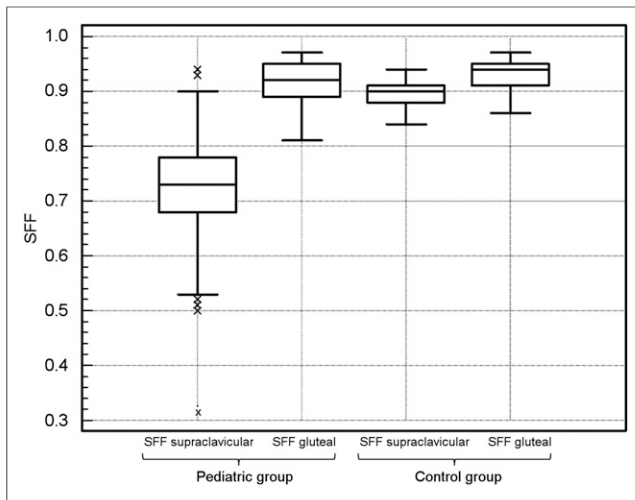
FIGURE 3. SFF in supraclavicular and gluteal fat depots in pediatric group compared with control group.

With regard to all pediatric patients (PET-positive and PET-negative subjects), SFF still differed significantly in supraclavicular fat depots compared with gluteal fat depots: mean supraclavicular SFF was 0.73 ± 0.1 (range, 0.32–0.94) and mean gluteal SFF was 0.91 ± 0.04 (range, 0.81–0.97), resulting in a P value of less than 0.0001.

In the control group ($n = 11$), mean SFF in supraclavicular fat depots was 0.90 ± 0.02 (range, 0.84–0.94). Mean SFF in gluteal depots was 0.93 ± 0.03 (range, 0.86–0.97). SFF in supraclavicular fat thus differed between pediatric subjects and the control group ($P < 0.0001$). No significant difference of the SFF in gluteal adipose tissue could be observed between pediatric and control subjects ($P = 0.13$). Remarkably, the range of the supraclavicular SFF in the control group was comparable to that of gluteal fat depots in the pediatric group (Fig. 3).
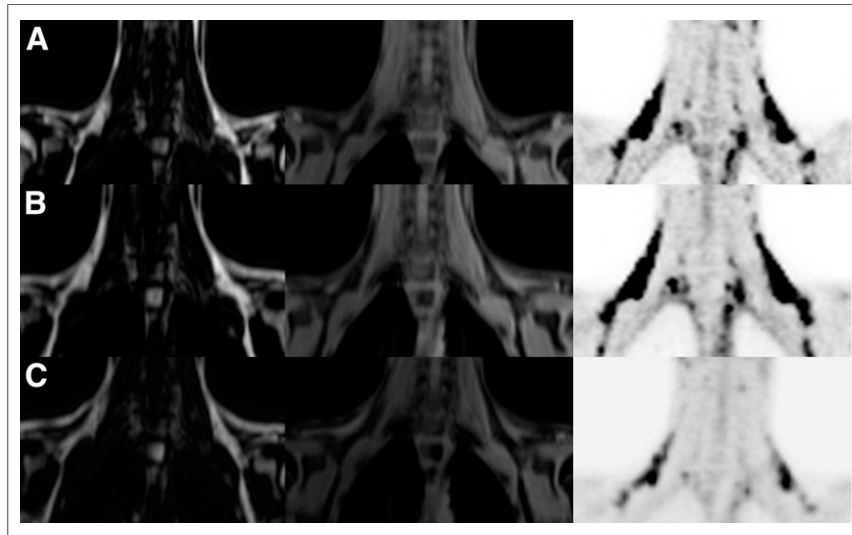
DISCUSSION

The results of the study indicate that SFF determined by the 2-point VIBE Dixon sequence is lower in BAT than WAT in children and that SFF is independent from the metabolic activity of the tissue as determined by ^{18}F-FDG PET. Thus SFF represents a robust parameter for the identification of BAT, suggesting that BAT can be identified using MR imaging only.

The results of the present study suggest that when a 2-point Dixon water–fat separation method is used, mean SFF in pediatric subjects is significantly lower in supraclavicular/cervical (brown) fat depots than gluteal subcutaneous (white) fat depots. This finding confirms that MR imaging with the described Dixon method is able to distinguish between these types of adipose tissue based on the higher water content of BAT (24,30) using a relatively fast 2-point Dixon water–fat separation method acquired for attenuation correction in simultaneous ^{18}F-FDG PET/MR imaging.

The advantage of using simultaneous ^{18}F-FDG PET/MR imaging in our study lies in the fact that the presence of BAT can be proven by showing metabolically active adipose tissue in ^{18}F-FDG PET and by evaluating the corresponding SFF at the same time. This simultaneous ^{18}F-FDG PET/MR imaging allowed an initial cross-validation of MR imaging with respect to its further use to distinguish between different types of adipose tissue (24,31). Consequently differences in SFF between gluteal and cervical adipose tissue in patients with metabolically active cervical fat can be attributed to the presence of different types of adipose tissue—that is, BAT and WAT.

Furthermore, with cervical and gluteal SFF values in PET-negative patients comparable to those in PET-positive patients and by prior validation of the use of SFF in PET-positive subjects to detect BAT, it can be concluded that in PET-negative patients BAT was also present in the cervical region, only not being metabolically active by the time of the examination. Consequently, BAT can possibly be detected by sole determination of the SFF via the 2-point Dixon water–fat separation method used in this study, even in patients without a positive PET signal.

In the control group composed of elderly subjects (≥ 76 y), supraclavicular SFF values were substantially higher than in the pediatric group, with ranges comparable to those in gluteal fat depots in both pediatric and elderly subjects (Fig. 3). Histologically, BAT was never shown to be present in gluteal fat (3,29), so it can be hypothesized that both the pediatric and the control group had WAT in gluteal fat depots. Consequently, the supraclavicular SFF range in the control group also points to WAT.

The reason for the statistically significant difference between supraclavicular and gluteal SFF in the control group is not completely clear. With regard to the range of supraclavicular and gluteal SFF in this population (Fig. 3), a broad overlap is present. It could be hypothesized that a minimal amount of BAT is still present in the supraclavicular region of elderly people, leading to a small but statistically significant drop of SSF. However, no histomorphologic data are available at the present.

FIGURE 4. (A–C) Images of patient C at 3 consecutive examinations (left, fat-weighted MR image; middle, water-weighted MR image; right, PET image). Black spots on PET image indicate metabolically active BAT. Note varying strength in PET signal (SFF at examination A, left/right, 0.70/0.74; B, 0.72/0.79; C, 0.75/0.78, and SUV_mean at examination A, left/right, 19.75/16.66; B, 16.09/18.25; C, 3.86/4.46).

With regard to the longitudinal analysis of SFF compared with ^{18}F-FDG PET, another crucial result of this study was that metabolic activity as determined by PET-based SUV analysis showed no correlation with SFF in subjects with metabolically active BAT. So far, it is not clear whether BAT is subject to short-term changes in metabolic activity (sleeping BAT), depending on factors such as nutritional status and environmental conditions (e.g., cold stimulation), or whether the human adipose organ is plastic, comparable to that of rodents in which adipocytes in BAT and WAT populations can reversibly turn into one another as short-term reaction to stimuli such as cold exposure (4,32,33).

When ^{18}F-FDG PET/CT is used, the detection of BAT is limited to the evidence of metabolic activity by a positive ^{18}F-FDG uptake in PET, with no further tissue characterization being possible. Thus, for tissue characterization in longitudinal studies with PET/CT, histology samples would be required, ideally sampled shortly after the PET/CT examination to avoid distortion by possible short-term plasticity of the adipose organ.

By using PET/MR imaging in the present study, it was possible to perform simultaneous measurements of metabolic activity as determined by SUV_{mean} and of accurately colocalized tissue composition as determined by SFF not being influenced by a potential change in the metabolic status and composition of BAT using sequential examinations. In subjects with multiple examinations, intraindividual SUV_{mean} fluctuated massively, with a median change of 91%, whereas intraindividual SFF was subject to only minor variations, with a median change of 5% (Fig. 2). These results indicate that the composition of the adipose tissue as determined by calculation of SFF stays relatively stable independent from the current metabolic activity (Fig. 4). Consequently, our data argue against the hypothesis of BAT being a plastic tissue and are in favor of its constant existence with only a different grade of metabolic activity. However, the hypothesis has to be proven in further studies. The present data suggest that BAT that is not detectable on PET images because of its metabolic inactivity can potentially be identified using SFF analysis.

The present study has some limitations. First, BAT can occur in mixed clusters with white adipocytes in humans (4,33); thus, a certain SFF range is suggestive only of the presence of BAT as it is an average value of the SFF within 1 fat depot. Furthermore, partial-volume effects have to be considered, especially when low-resolution PET data are used for setting the ROI, because SFF cannot differentiate between intracellular water content and nonlipid tissue portions (e.g., from vessels) within a voxel.

Second, SFF is not as accurate as the so-called PDFF. SFF refers to MR signal attributable to fat and is confounded by various MR imaging–related properties such as T1 or T2*; thus, values can differ when changing acquisition parameters, whereas PDFF refers to the fraction of mobile protons attributable to fat and removes biases such as T1 and T2* and is potentially more accurate because it uses multipeak fat spectral fitting (25). Water–fat separation methods applied on 6-echo gradient-echo data can extract PDFF and are thereby free of any confounding effects (31). Nevertheless, SFF based on a water–fat separation method applied on 2-echo gradient-echo data is a promising tool to verify the presence of BAT without radiation exposure as in PET. Thus, compared with PET, SFF and PDFF are more suited as a screening method for detecting BAT or as a method for longitudinal studies of fat distribution.

Third, the present study was limited by the predominantly male study population ($n = 24$), which was not intentional. Previous PET/CT studies provide conflicting information about sex dependence of BAT in pediatric cohorts (15,20), and further investigations should also determine sex effects on the presence and development of BAT.

Fourth, histology was not used as a gold standard diagnostic reference in differentiating WAT from BAT because of ethical and practical reasons. However, ^{18}F-FDG uptake is evidently related to metabolically active BAT (5,34). Furthermore, supraclavicular SFF in PET-positive and PET-negative pediatric patients were comparable and in both groups significantly different from gluteal subcutaneous WAT, which in turn was comparable to the supraclavicular and gluteal fat in the control subjects. Considering this together with results from autopsy studies (3), it can be assumed that BAT is present within the supraclavicular/cervical adipose tissue in pediatric subjects, and the different adipose tissue in pediatric subjects (gluteal) and elderly subjects (supraclavicular and gluteal) is WAT.

CONCLUSION

^{18}F-FDG PET/MR imaging is a promising tool for combined morphologic and functional evaluation of BAT, especially in the cross-validation of an MR technique for discrimination between WAT and BAT. The present preliminary data show that a 2-point Dixon sequence acquired for attenuation correction in ^{18}F-FDG PET/MR imaging can be used for reliable SFF analysis. Hereby, SFF represents a robust method for the differentiation of BAT and WAT being independent from the metabolic activation of BAT. The methods used in this study can potentially be applied in studies on human BAT in healthy cohorts and in longitudinal studies for monitoring BAT characteristics in response to stimulation and therapeutic interventions. Thus, further studies are promising and warranted, especially focusing on determining a reliable threshold between BAT and WAT for visualizing and evaluating BAT mass semiquantitatively. In addition, when information concerning the composition and extent of BAT and its specific activation status is needed, the use of MR imaging and PET by hybrid PET/MR imaging might provide supplemental information.

REFERENCES

1. Shabalina IG, Kramarova TV, Nedergaard J, Cannon B. Carboxyatractyloside effects on brown-fat mitochondria imply that the adenine nucleotide translocator isoforms ANT1 and ANT2 may be responsible for basal and fatty-acid-induced uncoupling respectively. *Biochem J.* 2006;399:405–414.
2. Enerbäck S. Human brown adipose tissue. *Cell Metab.* 2010;11:248–252.
3. Heaton JM. The distribution of brown adipose tissue in the human. *J Anat.* 1972;112:35–39.
4. Frontini A, Cinti S. Distribution and development of brown adipocytes in the murine and human adipose organ. *Cell Metab.* 2010;11:253–256.
5. Cypess AM, Lehman S, Williams G, et al. Identification and importance of brown adipose tissue in adult humans. *N Engl J Med.* 2009;360:1509–1517.
6. van Marken Lichtenbelt WD, Vanhommerig JW, Smulders NM, et al. Cold-activated brown adipose tissue in healthy men. *N Engl J Med.* 2009;360:1500–1508.
7. Virtanen KA, Lidell ME, Orava J, et al. Functional brown adipose tissue in healthy adults. *N Engl J Med.* 2009;360:1518–1525.
8. Betz MJ, Enerback S. Human brown adipose tissue: what we have learned so far. *Diabetes.* 2015;64:2352–2360.
9. Ogden CL, Carroll MD, Kit BK, Flegal KM. Prevalence of obesity and trends in body mass index among US children and adolescents, 1999-2010. *JAMA.* 2012;307:483–490.
10. Ghorbani M, Himms-Hagen J. Appearance of brown adipocytes in white adipose tissue during CL 316,243-induced reversal of obesity and diabetes in Zucker fa/fa rats. *Int J Obes Relat Metab Disord.* 1997;21:465–475.
11. Kim H, Pennisi PA, Gavrilova O, et al. Effect of adipocyte beta3-adrenergic receptor activation on the type 2 diabetic MKR mice. *Am J Physiol Endocrinol Metab.* 2006;290:E1227–E1236.

12. Himms-Hagen J, Cui J, Danforth E Jr, et al. Effect of CL-316,243, a thermogenic beta 3-agonist, on energy balance and brown and white adipose tissues in rats. *Am J Physiol.* 1994;266:R1371–R1382.

13. Bartelt A, Bruns OT, Reimer R, et al. Brown adipose tissue activity controls triglyceride clearance. *Nat Med.* 2011;17:200–205.

14. Vijgen GH, Bouvy ND, Teule GJ, Brans B, Schrauwen P, van Marken Lichtenbelt WD. Brown adipose tissue in morbidly obese subjects. *PLoS One.* 2011;6:e17247.

15. Drubach LA, Palmer EL, 3rd, Connolly LP, Baker A, Zurakowski D, Cypess AM. Pediatric brown adipose tissue: detection, epidemiology, and differences from adults. *J Pediatr.* 2011;159:939–944.

16. Boss O, Farmer SR. Recruitment of brown adipose tissue as a therapy for obesity-associated diseases. *Front Endocrinol (Lausanne).* 2012;3:14.

17. Nedergaard J, Bengtsson T, Cannon B. New powers of brown fat: fighting the metabolic syndrome. *Cell Metab.* 2011;13:238–240.

18. Bartelt A, Merkel M, Heeren J. A new, powerful player in lipoprotein metabolism: brown adipose tissue. *J Mol Med (Berl).* 2012;90:887–893.

19. Yoneshiro T, Aita S, Matsushita M, et al. Brown adipose tissue, whole-body energy expenditure, and thermogenesis in healthy adult men. *Obesity (Silver Spring).* 2011;19:13–16.

20. Gilsanz V, Smith ML, Goodarzian F, Kim M, Wren TA, Hu HH. Changes in brown adipose tissue in boys and girls during childhood and puberty. *J Pediatr.* 2012;160:604-609 e601.

21. Hu HH, Kan HE. Quantitative proton MR techniques for measuring fat. *NMR Biomed.* 2013;26:1609–1629.

22. van der Meer RW, Lamb HJ, Smit JW, de Roos A. MR imaging evaluation of cardiovascular risk in metabolic syndrome. *Radiology.* 2012;264:21–37.

23. Lunati E, Marzola P, Nicolato E, Fedrigo M, Villa M, Sbarbati A. In vivo quantitative lipidic map of brown adipose tissue by chemical shift imaging at 4.7 Tesla. *J Lipid Res.* 1999;40:1395–1400.

24. Hu HH, Perkins TG, Chia JM, Gilsanz V. Characterization of human brown adipose tissue by chemical-shift water-fat MRI. *AJR.* 2013;200:177–183.

25. Reeder SB, Cruite I, Hamilton G, Sirlin CB. Quantitative assessment of liver fat with magnetic resonance imaging and spectroscopy. *J Magn Reson Imaging.* 2011;34:spcone.

26. Chen YC, Cypess AM, Chen YC, et al. Measurement of human brown adipose tissue volume and activity using anatomic MR imaging and functional MR imaging. *J Nucl Med.* 2013;54:1584–1587.

27. Reddy NL, Jones TA, Wayte SC, et al. Identification of brown adipose tissue using MR imaging in a human adult with histological and immunohistochemical confirmation. *J Clin Endocrinol Metab.* 2014;99:E117–E121.

28. Dicker A, Ohlson KB, Johnson L, Cannon B, Lindahl SG, Nedergaard J. Halothane selectively inhibits nonshivering thermogenesis: possible implications for thermoregulation during anesthesia of infants. *Anesthesiology.* 1995;82:491–501.

29. Sacks H, Symonds ME. Anatomical locations of human brown adipose tissue: functional relevance and implications in obesity and type 2 diabetes. *Diabetes.* 2013;62:1783–1790.

30. Hu HH, Yin L, Aggabao PC, Perkins TG, Chia JM, Gilsanz V. Comparison of brown and white adipose tissues in infants and children with chemical-shift-encoded water-fat MRI. *J Magn Reson Imaging.* 2013;38:885–896.

31. Hu HH, Wu TW, Yin L, et al. MRI detection of brown adipose tissue with low fat content in newborns with hypothermia. *Magn Reson Imaging.* 2014;32:107–117.

32. Himms-Hagen J, Melnyk A, Zingaretti MC, Ceresi E, Barbatelli G, Cinti S. Multilocular fat cells in WAT of CL-316243-treated rats derive directly from white adipocytes. *Am J Physiol Cell Physiol.* 2000;279:C670–C681.

33. Cinti S. Transdifferentiation properties of adipocytes in the adipose organ. *Am J Physiol Endocrinol Metab.* 2009;297:E977–E986.

34. Hu HH, Tovar JP, Pavlova Z, Smith ML, Gilsanz V. Unequivocal identification of brown adipose tissue in a human infant. *J Magn Reson Imaging.* 2012;35:938–942.